Effect of air-loading on the performance limits of graphene microphones

Pezone, R.; Baglioni, G.; van Ruiten, C.; Anzinger, S.; Wasisto, H. S.; Sarro, P. M.; Steeneken, P. G.; Vollebregt, S.

DOI
10.1063/5.0191939

Publication date
2024

Document Version
Final published version

Published in
Applied Physics Letters

Applied Physics Letters

RESEARCH ARTICLE | MARCH 19 2024

Effect of air-loading on the performance limits of graphene microphones

R. Pezone ; G. Baglioni; C. van Ruiten ; S. Anzinger ; H. S. Wasisto ; P. M. Sarro ; P. G. Steeneken ; S. Vollebregt

Appl. Phys. Lett. 124, 123503 (2024)
https://doi.org/10.1063/5.0191939

AIP Publishing

Applied Physics Letters ARTICLE pubs.aip.org/aip/apl

Effect of air-loading on the performance limits of graphene microphones

Cite as: Appl. Phys. Lett. **124**, 123503 (2024); doi: 10.1063/5.0191939
Submitted: 17 December 2023 · Accepted: 6 March 2024 ·
Published Online: 19 March 2024

View Online Export Citation CrossMark

R. Pezone,[1] G. Baglioni,[2] C. van Ruiten,[3] S. Anzinger,[4] H. S. Wasisto,[4] P. M. Sarro,[1] P. G. Steeneken,[2,3] and S. Vollebregt[1,a)]

AFFILIATIONS

[1]Laboratory of Electronic Components, Technology and Materials (ECTM), Department of Microelectronics, Delft University of Technology, Mekelweg 4, 2628 CD Delft, The Netherlands
[2]Kavli Institute of Nanoscience, Department of Quantum Nanoscience, Delft University of Technology, Gebouwnummer 22, Lorentzweg 1, 2628 CJ Delft, The Netherlands
[3]Department of Precision and Microsystems Engineering (PME), Delft University of Technology, Mekelweg 2, 2628 CD Delft, The Netherlands
[4]Infineon Technologies AG, Am Campeon 1-15, Neubiberg 85579, Germany

[a)]**Author to whom correspondence should be addressed:** s.vollebregt@tudelft.nl

ABSTRACT

As a consequence of their high strength, small thickness, and high flexibility, ultrathin graphene membranes show great potential for pressure and sound sensing applications. This study investigates the performance of multi-layer graphene membranes for microphone applications in the presence of air-loading. Since microphones need a flatband response over the full audible bandwidth, they require a sufficiently high mechanical resonance frequency. Reducing membrane thickness facilitates meeting this bandwidth requirement, and therefore, also allows increasing compliance and sensitivity of the membranes. However, at atmospheric pressure, air-loading effects can increase the effective mass, and thus, reduce the bandwidth of graphene and other 2D material-based microphones. To assess the severity of this performance-limiting effect, we characterize the acoustic response of multi-layer graphene membranes with a thickness of 8 nm in the pressure range from 30 to 1000 mbar, in air and helium environments. A bandwidth reduction by a factor $\sim 2.8\times$ for membranes with a diameter of 500 μm is observed. These measurements show that air-loading effects, which are usually negligible in conventional microphones, can lead to a substantial bandwidth reduction in ultrathin graphene microphones. With analytical and finite element models, we further analyze the performance limits of graphene microphones in the presence of air-loading effects.

Graphene, and other 2D materials, hold significant promise in the MEMS (micro-electromechanical system) sensor field, thanks to their unique physical properties.[1] Several studies have explored the effect of pressure on the eigenfrequency of graphene membranes, resulting in large bandwidths up to tens of MHz.[2–4] Over the past 5 years, research has demonstrated that increasing the membrane size by using multi-layer graphene can further increase the potential for microphone and speaker applications, showcasing promising performance.[5–8] However, when increasing sensitivity, by reducing membrane tension or increasing membrane diameter, the resonance frequency and bandwidth of the microphones reduce. As a consequence of this trade-off, the only route toward higher performance is reducing the membrane thickness. However, when reducing the thickness of the membranes operating at atmospheric pressure, they become more susceptible to an air-loading effect that is called "added virtual mass increment" (AVMI) in the fluid–structure interaction literature.[9,10] Although this effective mass increase is negligible in most conventional microphones, we will demonstrate here that it can become a substantial factor in graphene microphones.

First, we will discuss the devices and experimental procedure. Second, we will characterize the frequency response of the devices as a function of pressure in both air and helium. Then, we will compare the experiments to AVMI theory and finally we will use models to analyze the implications for the performance limits of graphene microphones.

Free-standing multi-layer graphene membranes with an average thickness of 8 nm are grown on Si/SiO_2 (1000 nm)/Mo (50 nm) by a

low-pressure chemical vapor deposition process.[11] After releasing the graphene by etching the molybdenum sacrificial seed layer, the membranes are transferred on a silicon wafer with circular holes that are created by deep reactive ion etching.[5] These membranes are completely free from polymer residuals since no polymer supports have been used, which is relevant since the polymers are often a source of additional mass that can affect the membrane dynamics. As a result of the transfer approach, the membranes demonstrate differing pretension values for the same thickness (t_m) and radius (R).

In Fig. 1, an optical microscope image of a multi-layer membrane with a radius of 250 μm is shown. On the right of it, side-view and top-view images of the membrane by a scanning electron microscope (SEM) are shown. The top view image shows that the membranes contain small holes with diameters of less than 100 nm. We hypothesize that these holes might be formed during the graphene CVD process or after Mo etching and transfer, where weaker grains can be punched out. We estimate that these holes can help to prevent static pressure build-up across the membranes but are too small to have a substantial effect on the high-frequency acoustic response of the membranes.

The crystallinity of the multi-layer graphene is investigated using a Horiba HR800 Raman spectrometer featuring a 514.4 nm Ar+ laser and a 100× objective with a NA of 0.9. Figure S1 (supplementary material) displays the Raman signature of the multi-layer (ML) graphene.[6,12,13] The emergence of the D peak within the spectrum, with a ratio $I_D/I_G = 0.2$, is characteristic for the graphene growth process and is not linked to contamination or damage induced by the device fabrication procedure. An atomic force microscope (AFM) from Cypher Asylum Research is employed to determine the multi-layer graphene thickness of $t_m = 8$ nm in the air topography mode as in previous works.[5,6]

A schematic of the characterization setup is shown in Fig. 2. The eigenfrequency of the fundamental mode of the membrane is measured using a single-point laser Doppler vibrometer (LDV) setup, which includes a Polytec OFV-534 laser head and an MSA-500 decoder. The laser spot is focused on the membrane center, where the most significant displacement is expected for the fundamental mode. The motion is excited by a piezo-shaker positioned beneath the membrane that is driven by an AC voltage in the frequency band of interest. The experiments are performed inside a pressure controlled vacuum chamber over a pressure range of 30–1000 mbar. A Moku:Lab system generates the AC voltage and analyzes the LDV signal. A computer

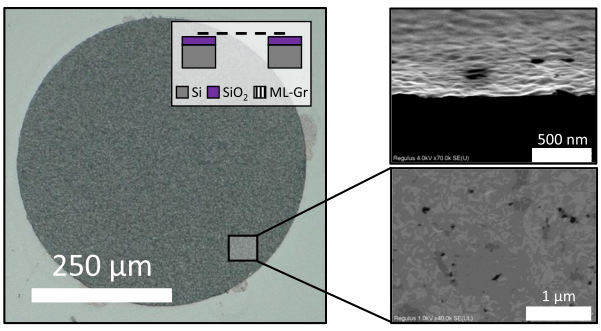

FIG. 1. Graphene membrane characterization. The optical microscope image of free-standing graphene with a radius $R = 250$ μm. The inset shows a top view of the membrane and a side view of a broken one.

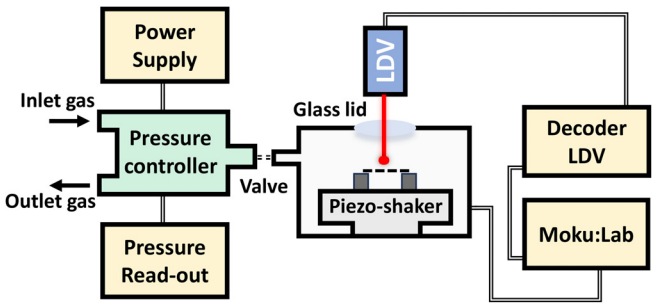

FIG. 2. Experimental setup. The schematic illustrates the experimental configuration, wherein the ML-Gr is actuated through a piezo-shaker controlled by an AC-voltage (frequency sweep) generated by a Moku:Lab system. The membrane frequency response is analyzed by a Laser Doppler Vibrometer that is connected to the Moku:Lab. A pressure controller is used to perform and monitor the upward pressure sweeps.

with python scripts is used to control all the experimental parameters and data acquisition via the Moku:Lab.

Figure 3(a) shows three measurements of the dependence of the fundamental resonance frequency f_{01} as a function of pressure for multi-layer graphene membranes with a radius of $R = 250$ μm and a thickness of $t_m = 8$ nm. Measurements B and C are performed on the same membrane in air and helium gas, while measurement A is performed in air on a membrane with a lower pretension. Figure 3(b) shows the frequency response data corresponding to case B in Fig. 3(a). This waterfall plot illustrates the variation in displacement magnitudes across the entire frequency spectrum (2–30 kHz) at different pressures (30–1000 mbar) for a membrane characterized by $n_0 = 0.007$ N/m.

In vacuum, the fundamental resonance frequency of a membrane is given by

$$f_{01} = \frac{2.405}{2\pi R}\sqrt{\frac{n_0}{\rho_m t_m}}. \tag{1}$$

For all three cases, the resonance frequency drops with increasing pressure, an effect that has not been observed experimentally in gases and cannot be accounted for by Eq. (1). However, the effect is well-known in the field of fluid–structure interactions,[9,10,14] where the resonance frequency of a plates and membranes in contact with a liquid is significantly reduced. The presence of the fluid, which is acoustically excited by the membrane, increases the effective inertia of the membrane.

The air-loading effect, thus, leads to an additional virtual mass, which is captured theoretically by the additional virtual mass index (AVMI) factor β that is given by

$$\beta = \Gamma\frac{\rho_f}{\rho_m}\frac{R}{t_m}, \tag{2}$$

where ρ_f is the density of the fluid or gas, ρ_m is the density of the membrane, and $\Gamma = 0.65$ is the nondimensional AVMI (NAVMI) factor for the fundamental resonance mode for a clamped circular plate.[9,10] Thus, in the presence of air, the effective mass density of the membrane increases by a factor $1 + \beta$ resulting in a pressure dependent resonance frequency $f_{01}(P)$,

$$f_{01}(P) = \frac{2.405}{2\pi R}\sqrt{\frac{n_0}{\rho_m t_m + \rho_f(P)R}}, \tag{3}$$

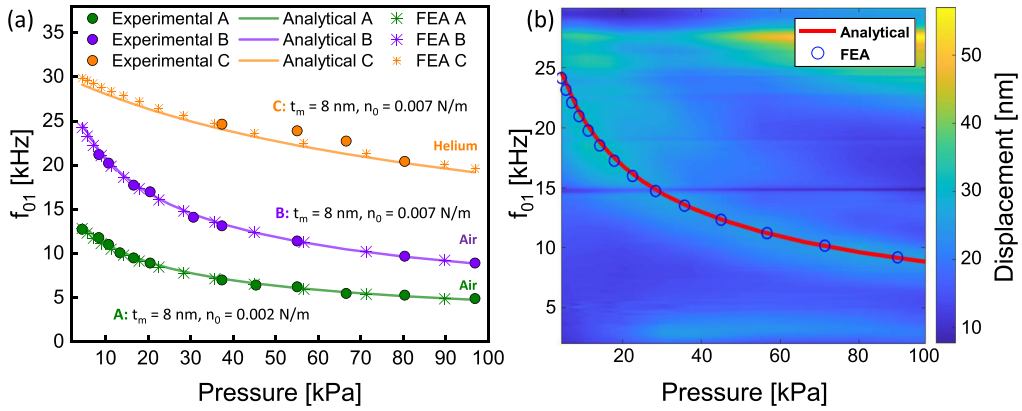

FIG. 3. Frequency reduction in f_{01} as a function of increasing pressure due to the air-loading effect. Three measurements are performed on ML-Gr membranes with $R = 250\ \mu$m and $t_m = 8$ nm. Membranes A and B are measured in air, and membrane C is a measurement of the same membrane as in B in helium gas. The reported results exclude experimental data points (case C) above 25 kHz due to the limitations of the piezoelectric transducer used in our experiments. Note that the lowest pressure plotted is 3 kPa. Lines and stars represent analytical and finite element simulation results based on the "Multiphysics" physics that couples the "Thermoviscous Acoustics, Frequency Domain" and "Membrane" modules. (b) Waterfall plot presenting results from membrane B in air.

where the pressure dependent gas density is given by $\rho_f(P) = \frac{P}{C_p T}$ and C_p is the specific heat capacity of the gas with $C_{p,helium} = 2076.9$ J/(kg K) and $C_{p,air} = 287.5$ J/(kg K).

To validate the hypothesis that the resonance frequency reduction is due to air-loading, we plot Eq. (3) as solid lines in Fig. 3 and also include Comsol finite element method (FEM) results. The good agreement between simulations and measurements, both in air and helium gas, give us confidence that the observed effects are, indeed, due to a large effective mass enhancement by air-loading, leading to a resonance frequency reduction of more than a factor of 2. We note that since $\Gamma\rho_f/\rho_m = 4.6 \times 10^{-5}$ is very small for air and graphene, the factor β from Eq. (2) is often small, such that air-loading is too insignificant to be observed. We observe it here because of the large aspect ratio $R/t_m = 31\ 250$ of the membrane that is enabled by the low thickness of graphene. In addition to the virtual mass increase due to the air-loading, we note that air-damping can also affect the resonance frequency and bandwidth of microphones. In a simplified mass–spring–damper model, the damped resonance f_d can be estimated as follows:

$$f_d = f_{01}\sqrt{1 - \frac{1}{4Q^2}}. \tag{4}$$

Considering the lowest Q-factor measured for sample A ($Q = 1.92$) at ≈1000 mbar, it follows from Eq. (4) that this damping will lead to a maximum decrease in bandwidth f_d of 4%, which is substantially smaller than total frequency shift observed in Fig. 3.

Additionally, it is important to highlight that condenser microphones are coupled with a read-out circuit as application-specific integrated circuit (ASIC), providing a constant bias voltage (V_{bias}) to the electrodes. This V_{bias} introduces electrostatic forces, leading to "electrostatic softening," which notably decreases the resonance frequency, further influencing the dynamic response of the system.

After having established the relevance of air-loading for the performance of graphene microphones, we now use models to estimate the effects on the ultimate performance of these membranes. Assuming that we have a fabrication method to adjust the pretension freely, we adjust it to a value $n_{20\text{kHz}}$ to satisfy the requirement that the resonance frequency of the membrane is $f_{01}(1000\ \text{mbar}) = 20$ kHz, to ensure that the bandwidth of the microphone is large enough to cover the full audible band. Using Eqs. (1) and (3), we calculate and plot in Fig. 4(a) the resulting pre-tension $n_{20\text{kHz}}$ for graphene membranes of different radius R and thickness t_m.

Notably, as evident from the difference between the curves with (continuous lines) and without air-loading (dashed lines), the influence of air-loading becomes more apparent for larger radii and thinner thicknesses. From these pre-tension values that are set by the bandwidth requirement, we can now assess in Fig. 4(b) the mechanical compliance and sensitivity of the membrane. The linear compliance S_m of a circular membrane is defined as the average membrane deflection divided by the pressure difference across the membrane and is given by $S_m = R^2/(8n_0)$ and is called the mechanical sensitivity[5,15] of the microphone. Thus, using the pre-tension values from the curves in (a), the sensitivity of the graphene membranes in the presence of air-loading in Fig. 4(b) is plotted using

$$S_{\text{m,20 kHz}} = \frac{R^2}{8n_{20\,\text{kHz}}} = \frac{2.405^2}{32\pi^2 \cdot (20\,\text{kHz})^2\left(\rho_m t_m + \frac{P_{air}R}{C_p T}\right)}. \tag{5}$$

An interesting observation from Fig. 4(b) is that for a higher thickness or in the absence of air-loading, the sensitivity $S_{\text{m,20kHz}}$ is independent of the membrane radius, because $n_0 \propto R^2$ to ensure a constant resonance frequency according to (1), while Eq. (5) causes $S_m \propto n_0/R^2 = \text{const}$. Reducing the membrane thickness increases the sensitivity up to the point where air-loading limits further improvement and we have in the small thickness limit that $S_{\text{m,20kHz}} = \left(\frac{2.405}{2\pi 20\text{kHz}}\right)^2 \frac{C_p T}{8P_{air}R}$. Since the AVMI factor $\beta \propto \frac{R}{t_m}$, this point is reached at higher thickness for large radius membranes, and therefore, the maximum achievable sensitivity S_m is highest for the small radius membranes in Fig. 4(b).

However, despite their potential record sensitivity, there is a drawback to making the membranes small: small membranes become

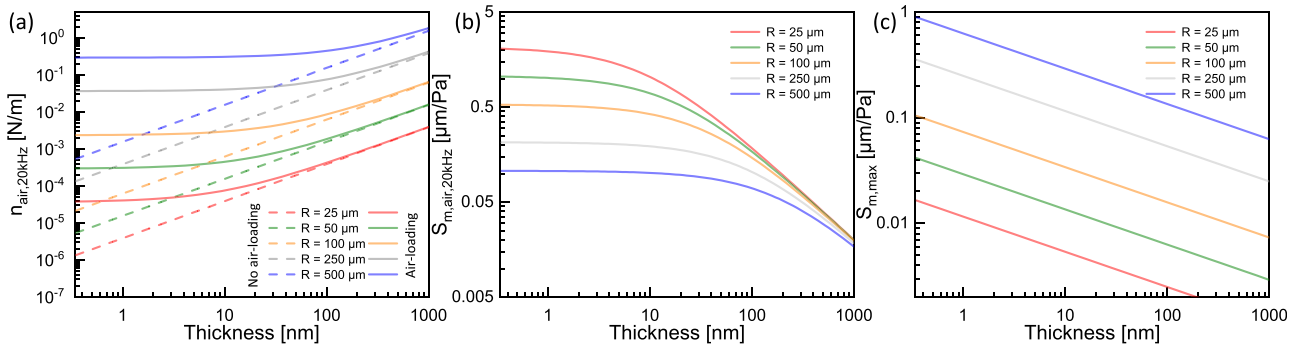

FIG. 4. Pre-tension and sensitivity for flat audible bandwidth based on the proposed analytical model. (a) Minimum pre-tensions required to achieve a flat bandwidth within the maximum audible frequency range ($f_{01} = 20$ kHz), considering different radii and thicknesses. The results are presented both with and without the air-loading effect. (b) The maximum mechanical sensitivity at atmospheric pressure is shown in accordance with the findings presented in (a), using Eq. (5). (c) To limit the nonlinearities in the pressure–deflection response, the amplitude at the maximum operation pressure should be constrained. This constraint also limits the maximum mechanical sensitivity $S_{m,max}$, which is plotted here for different graphene membrane geometries, for $\alpha = 0.1$ and $\Delta P_{max} = 1$ Pa.

mechanically nonlinear earlier under high pressure. This causes them to become less sensitive and results in harmonic distortion when sound pressure levels become high. The mechanical nonlinearity is given by this following equation:[16,17]

$$\Delta P = \frac{4n_0}{R^2}z + \frac{8Et_m}{3R^4(1-\nu)}z^3 = \Delta P_{\mathrm{lin}} + \Delta P_{\mathrm{nl}}, \tag{6}$$

where E is the Young's modulus and ν is the Poisson's ratio of the membrane material. To prevent substantial nonlinearities from occurring at a maximum operating sound pressure ΔP_{max}, one needs to keep the center deflection z smaller than a limiting value z_{lim}, such that the pressure from the z^3 nonlinear term stays smaller by a factor $\alpha = \Delta P_{\mathrm{nl}}/\Delta P_{\mathrm{lin}}$ than the linear term. Then, we obtain for small α (we use $\alpha = 0.1$), a limit to the amplitude and sensitivity:

$$z_{\mathrm{lim}} = \sqrt{\alpha\frac{3R^4(1-\nu)}{16Et_mS_{\mathrm{m}}}}, \tag{7}$$

$$\Delta P_{\mathrm{max}} \approx z_{\mathrm{lim}}/(2S_{\mathrm{m}}), \tag{8}$$

$$S^3_{\mathrm{m,max}} \approx \frac{3\alpha R^4(1-\nu)}{(8\Delta P_{\mathrm{max}})^2 Et_m}. \tag{9}$$

So, besides the limit on the sensitivity set by the bandwidth limitation of 20 kHz, there is another sensitivity limit set by the maximum allowable nonlinearity α of the response at the maximum operating pressure ΔP_{max}, given by (9) which we plot in Fig. 4(c) with $\Delta P_{\mathrm{max}} = 1$ Pa, and $E = 1$ TPa, $\nu = 0.16$ for graphene. It is seen that whereas the maximum sensitivity reached by small membranes is highest in Fig. 4(b), the sensitivity of large membranes is highest in Fig. 4(c). So an optimum radius can be found that is a compromise between bandwidth, sensitivity, and nonlinear distortion performance. Making the membrane thinner, however, tends to be beneficial in general, although it might affect robustness and manufacturability.

Let us finally estimate this robustness, considering that there is a maximum yield strain[16] $\varepsilon_y = \frac{2}{3}z_y^2/R^2$ of the material, which was found to be $\varepsilon_y = 0.012$ for graphene,[18] such that the maximum deflection the membrane can sustain (neglecting pretension) is $z_y = R\sqrt{1.5\varepsilon_y}$, which corresponds to a maximum yield pressure $\Delta P_y = 8Et_mz_y^3/[3R^4(1-\nu)]$ obtaining

$$\Delta P_y = \frac{\sqrt{24}Et_m\varepsilon_y^{3/2}}{R(1-\nu)}. \tag{10}$$

Thus, for a graphene membrane that should survive a pressure difference of $\Delta P_y = 10^5$ Pa, the aspect ratio of the membrane should stay lower than $R/t_m < 76 \times 10^3$. For the membranes under study, we have $R/t_m = 31.5 \times 10^3$ and satisfy this requirement.

In addition to the previously discussed considerations regarding the maximum yield pressure (ΔP_{max}), we conducted pressure robustness tests on four membranes. These membranes, each based on the same multi-layer graphene with a radius (R) of 350 μm, were subjected to static pressure applied through a nozzle corresponding to each membrane. The observed pressure robustness values were 1×10^5, 0.86×10^5, 0.4×10^5, and 0.64×10^5 Pa.

It is notable that these values are lower than the estimated maximum yield pressure (ΔP_y) based on Eq. (10), which is expected to be $\Delta P_y = 1.75 \times 10^5$ Pa. This discrepancy may be attributed to variations in the maximum yield strain and Young's modulus of the multi-layer graphene employed in this work. The mechanical properties of the material are notably influenced by the synthesis method employed and different clamping geometries.[19] Furthermore, the presence of holes, as illustrated in Fig. 1, could potentially contribute to a further reduction in the maximum yield pressure of the proposed membranes compared to the value predicted by Eq. (10).

In conclusion, in this work, we experimentally examine the effects of the air-loading on the sensitivity of multi-layer graphene membranes and present both analytical and FEM models to account for the observed pressure dependence of the resonance frequency, based on the AVMI factor. The study reveals that air-loading can significantly alter the resonance frequency, with observed reduction in the resonance frequency of more than a factor of 2 with respect to the vacuum value. Using the experimentally validated model, the research also puts forth an estimate for the maximum mechanical sensitivity for multi-layer graphene microphones, including bandwidth constraints and effects of air-loading. A short analysis of the limitations posed by nonlinear mechanics of the membrane is also presented, leading to an overall conclusion that reducing the membrane thickness is in general favorable for increasing the microphone sensitivity, although below a certain thickness further improvement is limited by the air-loading

effect. For the radius of microphone membranes, the situation is less straightforward, and an optimum radius needs to be determined from a trade-off between linearity, bandwidth, and other device parameters, such as capacitance, electrical sensitivity, and pull-in voltages requirements. Thus, this work provides a framework of equations than can facilitate multi-objective optimization of microphone membranes for operation close to their performance limits.[20]

See the supplementary material for details regarding Raman characterization (PDF 1) (S1) and Comsol modeling (PDF 1) (S2).

The authors thank the Delft University of Technology Else Kooi Lab staff for processing support. This project has received funding from European Union's Horizon 2020 research and innovation program under Grant Agreement No. 881603 (Graphene Flagship).

AUTHOR DECLARATIONS

Conflict of Interest

The authors have no conflicts to disclose.

Author Contributions

Roberto Pezone: Data curation (equal); Formal analysis (equal); Investigation (supporting); Writing – original draft (lead); Writing – review & editing (lead). **Gabriele Baglioni:** Conceptualization (equal); Methodology (equal); Supervision (supporting). **Cas van Ruiten:** Conceptualization (equal); Data curation (equal); Formal analysis (equal); Investigation (equal); Methodology (equal). **Sebastian Anzinger:** Writing – review & editing (supporting). **Hutomo Suryo Wasisto:** Writing – review & editing (supporting). **Pasqualina Maria Sarro:** Resources (equal); Writing – review & editing (supporting). **Peter Steeneken:** Conceptualization (equal); Funding acquisition (equal); Project administration (equal); Supervision (equal); Writing – review & editing (equal). **Sten Vollebregt:** Funding acquisition (equal); Project administration (equal); Resources (equal); Writing – review & editing (supporting).

DATA AVAILABILITY

The data that support the findings of this study are available from the corresponding author upon reasonable request.

REFERENCES

[1]M. C. Lemme, S. Wagner, K. Lee, X. Fan, G. J. Verbiest, S. Wittmann, S. Lukas, R. J. Dolleman, F. Niklaus, H. S. J. van der Zant, G. S. Duesberg, and P. G. Steeneken, "Nanoelectromechanical sensors based on suspended 2D materials," Research **2020**, 8748602.

[2]R. J. Dolleman, D. Davidovikj, S. J. Cartamil-Bueno, H. S. van der Zant, and P. G. Steeneken, "Graphene squeeze-film pressure sensors," Nano Lett. **16**, 568–571 (2016).

[3]A. Keşkekler, H. Arjmandi-Tash, P. G. Steeneken, and F. Alijani, "Symmetry-breaking-induced frequency combs in graphene resonators," Nano Lett. **22**, 6048–6054 (2022).

[4]P. G. Steeneken, R. J. Dolleman, D. Davidovikj, F. Alijani, and H. S. J. van der Zant, "Dynamics of 2D material membranes," 2D Mater. **8**, 042001 (2021).

[5]G. Baglioni, R. Pezone, S. Vollebregt, K. C. Zobenica, M. Spasenović, D. Todorović, H. Liu, G. J. Verbiest, H. S. J. van der Zant, and P. G. Steeneken, "Ultra-sensitive graphene membranes for microphone applications," Nanoscale **15**, 6343–6352 (2023).

[6]R. Pezone, G. Baglioni, P. M. Sarro, P. G. Steeneken, and S. Vollebregt, "Sensitive transfer-free wafer-scale graphene microphones," ACS Appl. Mater. Interfaces **14**, 21705–21712 (2022).

[7]S. Wittmann, C. Glacer, S. Wagner, S. Pindl, and M. C. Lemme, "Graphene membranes for hall sensors and microphones integrated with CMOS-compatible processes," ACS Appl. Nano Mater. **2**, 5079–5085 (2019).

[8]R. Pezone, S. Anzinger, G. Baglioni, H. S. Wasisto, P. M. Sarro, P. G. Steeneken, and S. Vollebregt, "Highly-sensitive wafer-scale transfer-free graphene MEMS condenser microphones," Microsyst. Nanoeng. **10**, 27 (2024).

[9]M. Kwak and K. Kim, "Axisymmetric vibration of circular plates in contact with fluid," J. Sound Vib. **146**, 381–389 (1991).

[10]M. Amabili, G. Frosali, and M. Kwak, "Free vibrations of annular plates coupled with fluids," J. Sound Vib. **191**, 825–846 (1996).

[11]S. Vollebregt, B. Alfano, F. Ricciardella, A. Giesbers, Y. Grachova, H. Van Zeijl, T. Polichetti, and P. M. Sarro, "A transfer-free wafer-scale CVD graphene fabrication process for MEMS/NEMS sensors," in *IEEE 29th International Conference on Micro Electro Mechanical Systems (MEMS)* (IEEE, 2016), pp. 17–20.

[12]N. B. Babaroud, M. Palmar, A. I. Velea, C. Coletti, S. Weingärtner, F. Vos, W. A. Serdijn, S. Vollebregt, and V. Giagka, "Multilayer CVD graphene electrodes using a transfer-free process for the next generation of optically transparent and MRI-compatible neural interfaces," Microsyst. Nanoeng. **8**, 107 (2022).

[13]F. Ricciardella, S. Vollebregt, T. Polichetti, M. Miscuglio, B. Alfano, M. L. Miglietta, E. Massera, G. D. Francia, and P. M. Sarro, "Effects of graphene defects on gas sensing properties towards NO_2 detection," Nanoscale **9**, 6085–6093 (2017).

[14]H. Lamb, "On the vibrations of an elastic plate in contact with water," Proc. R. Soc. London, Ser. A **98**, 205–216 (1920).

[15]P. Scheeper, A. Van der Donk, W. Olthuis, and P. Bergveld, "A review of silicon microphones," Sens. Actuators A **44**, 1–11 (1994).

[16]R. Dolleman, "Graphene based pressure sensors: Resonant pressure transduction using atomically thin materials," M.S. thesis, Delft University of Technology, 2014.

[17]J. S. Bunch, "Mechanical and electrical properties of graphene sheets," Ph.D. thesis (Cornell University, 2008).

[18]M. Goldsche, J. Sonntag, T. Khodkov, G. J. Verbiest, S. Reichardt, C. Neumann, T. Ouaj, N. von den Driesch, D. Buca, and C. Stampfer, "Tailoring mechanically tunable strain fields in graphene," Nano Lett. **18**, 1707–1713 (2018).

[19]A. Castellanos-Gomez, V. Singh, H. S. J. van der Zant, and G. A. Steele, "Mechanics of freely–suspended ultrathin layered materials," Ann. Phys. **527**, 27–44 (2014).

[20]H. Saheban, Z. Kordrostami, and S. Hamedi, "A multi-objective optimization of sensitivity and bandwidth of a 3-D MEMS bionic vector hydrophone," Analog Integr. Circuits Signal Process. **110**, 455–467 (2022).